Materials and Design 80 (2015) 152–162

Contents lists available at ScienceDirect

Materials and Design

journal homepage: www.elsevier.com/locate/matdes

The effect of undercooling on the microstructure and tensile properties of hypoeutectic Sn–6.5Zn–*x*Cu Pb-free solders

A.A. El-Daly [a,b,*], W.M. Desoky [a], A.F. Saad [a], N.A. Mansor [a], E.H. Lotfy [a], H.M. Abd-Elmoniem [a], H. Hashem [a]

[a] Physics Department, Faculty of Science, Zagazig Univ., Zagazig, Egypt
[b] Center of Nanotechnology, Zagazig Univ., Zagazig, Egypt

ARTICLE INFO

Article history:
Received 11 January 2015
Revised 4 May 2015
Accepted 6 May 2015
Available online 9 May 2015

Keywords:
Lead-free solders
Hypoeutectic Sn–6.5Zn alloy
Microstructure
Mechanical properties

ABSTRACT

Hypoeutectic Sn–6.5Zn alloy may be regarded as a better choice than eutectic Sn–9Zn lead-free solder in microelectronics industry. In this study, the properties of hypoeutectic Sn–6.5Zn lead-free solder were modified with minor additions of Cu. SEM investigations reveal that the plain Sn–6.5Zn solder exhibits large number of undesirable acicular structure of angular needle-like Zn particles at the solder matrix. The acicular-shape morphology of Zn was remarkably suppressed after Cu modification. Moreover, a new type of small flower-like γ-Cu_5Zn_8 intermetallic compound (IMC) was detected with 0.5 wt.% Cu added specimens. The flower-like morphology of γ-Cu_5Zn_8 IMC appears to cause a sharp increase in Young's modulus, yield strength (YS) and ultimate tensile strength (UTS) of Cu modified solder. However, this effectiveness is reduced when 1.5 wt.% Cu addition starts to enhance the growth of coarse dendrite morphology of γ-Cu_5Zn_8 phase with enlarged β-Sn matrix. In addition, a 1.5 wt.% Cu addition was found to induce undesirable effects on the degree of undercooling, melting temperature and pasty range. Constitutive Garofalo model was assembled based on the experimental data of Sn–6.5Zn lead-free solders.

1. Introduction

Low temperature solders have been extensively used in microelectronics packaging industry for many decades [1]. The growing focus on high performance and miniaturization has generated an urgent need to develop high-performance lead-free solder alloy for package quality and reliability [2,3]. This creates the demanding issue of producing reliable solder alloys with better mechanical properties and low cost. Therefore, understanding both the solders and processing aspects are crucial for manufacture sound electronic products without any serious problems. Among the novel lead-free solders, the eutectic Sn–9Zn system has been considered as one of the most attractive lead-free solders owing to its excellent mechanical properties, low melting temperature (198 °C), significant benefit on cost and other comprehensive performances [4]. Even though these alloys can be applied to a wide variety of applications, the poor wetting characteristics and poor oxidation resistance, which may be attributed to the higher surface tension and oxidation sensitivity of Zn, still limit the adoption of these alloys to certain applications [5]. The adequate characterization of mechanical behavior of solder alloys is one of the key issues to address, in order to gain deformation data on small solder joints. One innovative, potentially viable and economically affordable approach, to enhance the oxidation resistance and improve the mechanical properties of eutectic Sn–Zn solder is the addition of an appropriate secondary phase for the formation of Zn-based IMCs [6,7]. Another approach is the reduction of Zn content in alloy matrix [8]. According to Sn–Zn equilibrium phase diagram [8], reducing Zn content near the hypoeutectic Sn–6.5Zn composition will remain the equilibrium eutectic melting point at the same level. Notably, some researchers have started to focus on the above weakness points, which are still the main challenging issue for the packaging industry. For instance, Wei et al. [9] carried out the thermal tests for hypoeutectic Sn–6.5Zn and eutectic Sn–9Zn alloys. It was found that the Sn–6.5Zn can behave in the same way as the eutectic Sn–9Zn during melting, although it has remarkably better wettability to Cu than Sn–9Zn solder. They also proposed that Sn–6.5Zn can be used as a lead-free solder, while mostly keeping its benefit of generating the same eutectic temperature of Sn–9Zn alloy. Apart from its favorable melting temperature and wettability, the microstructures and mechanical properties of hypoeutectic Sn–4 wt.% Zn alloy, hypereutectic Sn–12 wt.% Zn alloy and eutectic Sn–9 wt.% Zn alloy were examined by Garcia et al. [6]. The microstructure of eutectic Sn–9 wt.% Zn alloy induced higher

* Corresponding author at: Physics Department, Faculty of Science, Zagazig Univ., Zagazig, Egypt.
E-mail addresses: dreldaly11@yahoo.com, dreldaly@zu.edu.eg (A.A. El-Daly).

http://dx.doi.org/10.1016/j.matdes.2015.05.016
0261-3069/

mechanical strength than those of Sn–4 wt.% Zn and Sn–12 wt.% Zn alloys owing to the formation of globular Zn-rich phase in the former. However, requirements such as high mechanical strength and creep resistance are of prime importance for the selection of alternative solder alloys. In a recent study [10,11], the as-cast microstructure of Ni and Sb-containing Sn–6.5Zn solder was characterized. The resulting thermal behavior and mechanical strength were also determined. It was established that the enhanced solid solution effect of Sb and the flower-like shaped $(Ni, Zn)_3Sn_4$ IMC phase produced by Ni addition play an important role on the melting temperature, undercooling and the mechanical strength of new solders. The amount of undercooling is reduced, while the melting temperature and pasty range remained at the hypoeutectic Sn–6.5Zn level. Microstructural analysis also revealed that the enhanced solid solution effect of Sb and the flower shaped $(Ni, Zn)_3Sn_4$ IMC phase are beneficially effective in reducing the creep rate of Ni and Sb-containing Sn–6.5Zn solders [11]. The creep resistance of Sn–6.5Zn solder was enhanced to about ~270% and ~182% with the addition of with Ni and Sb, respectively. In the present study, the influence of small amounts of Cu on the microstructural evolution and thermal behavior of Sn–6.5Zn solder were investigated. In addition, the mechanical properties of these Sn–6.5Zn–*x*Cu alloys were measured depending on the content of Cu additions.

2. Experimental procedures

Commercially pure elements of Sn (99.9%), Zn (99.99%) and Cu (99.99%) were used to elaborate the proposed solder alloys. Composition of solder alloys were Sn–6.5Zn, Sn–6.5Zn–0.5 wt.% Cu and Sn–6.5Zn–1.5 wt.% Cu alloys. The process of melting was carried out in a vacuum arc furnace under protection of high purity argon atmosphere at 800 °C for about 1 h. In order to get a homogeneous composition within the ingots, the alloy samples were re-melted three times to produce rod-like specimen with a diameter of about 1.5 cm. The chemical compositions of casted alloys were analyzed using inductive coupled plasma-optical emission spectrometry (ICP-OES, model: Optima 5300DV, Perkin Elmer). The results are given in Table 1. Morphology and composition of IMCs in the solder alloys were analyzed by Scanning Electron Microscopy (SEM) (FE-SEM, model: S-4800, HITACHI) in backscattered electron (BSE) mode. IMCs and phases were conducted by Energy Dispersive X-ray Spectrometry (EDS). A solution of 3%HCl, 2%HNO_3 and 95% (vol.%) ethyl alcohol was prepared and used to etch the samples. Phase identification of the alloy samples were carried out by X ray diffractometry (XRD) at 40 kV and 20 mA using Cu Kα radiation with diffraction angle from 25° to 90° and a constant scanning speed of 1° min^{-1}. Differential scanning calorimetry (Shimadzu DSC-50) was carried out to identify the melting process of three solder alloys. Heating and cooling rates in DSC analysis were carried out at 10 °C/min in Ar flow. Characterization of constitutive alloy behavior is generally done through tensile tests using standard specimens. Such samples are usually manufactured from standard bar-solder, which is melted and solidified in a steel mold. In order to obtain relevant constitutive data for real interconnections, specimens had to be scaled down to a typical solder joint size if one considers the extremely small solder volumes in modern microelectronic industry [12,13]. Therefore, the design optimization of solder joints could be conducted with different geometries to investigate the tensile behavior. In the present work, the homogenized cast ingots were then mechanically machined into a wire samples with a gauge length marked 4×10^{-2} m for each samples and 1.2 mm diameter (see Fig. 1). Details are described in [14]. The small sized solder specimens used in this work had more advantageous than the test standards since the tensile behavior follows a simple power law. Besides, the metallization material changes not only the absolute tensile strength, but also the stress sensitivity (stress exponent) of the tensile behavior. Such effects could not be found in bulk specimens. Before testing, the specimens were annealed at 120 °C for 45 min to reduce the residual stress induced during sample preparation. Then, tensile properties were characterized using a computerized tensile testing machine described elsewhere [15] at temperature range of 25–110 °C. The tensile tests also were carried out at various strain rates ranging from 10^{-5} to 10^{-3} s^{-1} and constant temperature of 25 °C. The axial strain is measured in accordance with the Active Standard ASTM E8/E8M, and ASTM E1012/E466 Practice standard for force verification. Then, the mechanical properties were obtained by averaging three testing data. The environment chamber temperature could be monitored by temperature control using a thermocouple contacting with specimen.

3. Results and discussion

3.1. Thermal behavior

The melting temperature and undercooling processes of solder alloys are a crucial factors that have to be taken into account in order to maintain high electronic packaging quality. To simulate the cooling rates of ball-grid array (BGA), the thermal behavior of three solder alloys was quantified using DSC analysis at 10 °C/min. The results are shown in Fig. 2 and summarized in Table 2. For Sn–6.5Zn and Sn–6.5Zn–0.5Cu solders, only one endothermal peak (T_m) emerged at 200.5 °C and 200.6 °C, respectively, although two endothermal peaks were detected for Sn–6.5Zn–1.5Cu solder at 200.6 and 214.6 °C, which indicate a strong dependence of T_m on the amount of Cu addition. The Sn–Zn equilibrium diagram [8] is given in Fig. 3. However, as can be seen from Sn–Zn binary diagram, the peak around 200.6 °C is due to the second-phase formation in solder matrix, while the β-Sn primary phase melts at 214.6 °C. Actually, these results completely agree with that reported by El-Daly et al. [11,12], where the same effect

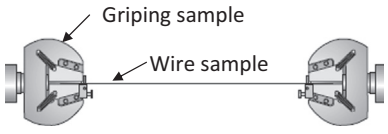

Fig. 1. Schematic diagram of tensile specimens as well as the griping of samples on the testing machine (wire samples with a gauge length marked 4×10^{-2} m and 1.2 mm diameter).

Table 1
Chemical composition of three solders studied (wt.%).

Alloy	Cu	Si	Fe	As	Pb	Zn	In	Sn
Sn–6.5Zn	0.000	0.008	0.001	0.002	0.001	6.510	0.004	Bal.
Sn–6.5Zn–0.5Cu	0.506	0.009	0.001	0.002	0.001	6.523	0.004	Bal.
Sn–6.5Zn–1.5Cu	1.504	0.009	0.001	0.002	0.001	6.521	0.004	Bal.

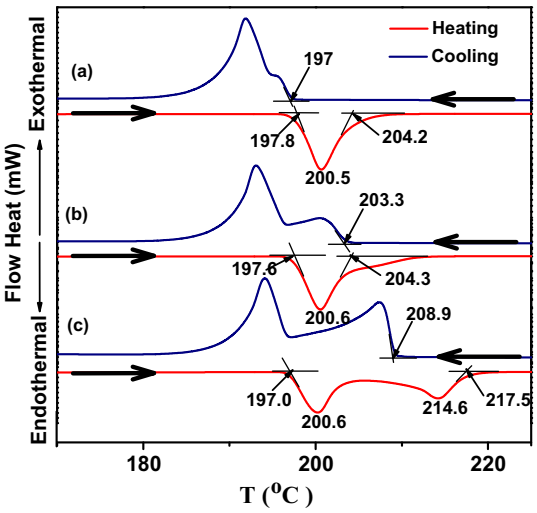

Fig. 2. DSC results of (a) Sn–6.5Zn, (b) Sn–6.5Zn–0.5Cu and (c) Sn–6.5Zn–1.5Cu solder alloys during heating (endothermal) and cooling (exothermal).

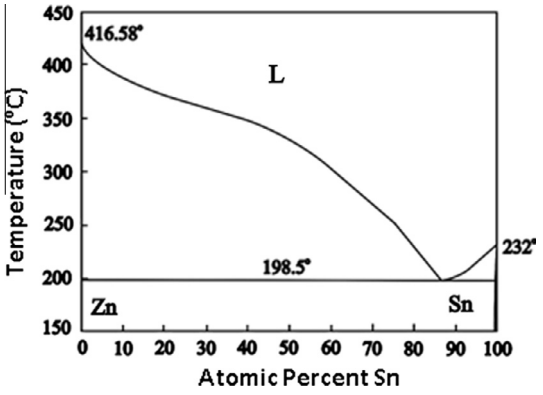

Fig. 3. Sn–Zn phase diagram [9].

has been established with the addition of small amounts of Ni and Sb into Sn–6.5Zn solder alloy. However, the pasty range is defined as:

$$\text{Pasty range} = T_{\text{end}} - T_{\text{onset}} \quad (1)$$

where T_{end} is the liquidus temperature and T_{onset} is the solidus temperature during heating.

For Sn–6.5Zn and Sn–6.5Zn–0.5Cu solders, the pasty range lies in the range of 6.4–6.7 °C, which is lower than 11.5 °C for Sn–Pb solders [10,11]. With increasing Cu content, the pasty range increases to 20.5 °C. Large pasty range detected in Sn–6.5Zn–1.5Cu solder may result in many manufacturing problems, such as increasing the tendency toward porosity, promote the probability of fillet lifting phenomena and hot tearing tightening during solidification [14].

In most cases of solidification process, the molten solder is cooled too quickly to permit the equilibrium phases to form. However, the starting points of melting and solidification of solders are essential processes in real soldering process of electronic packaging. Accordingly, the amount of undercooling ΔT can be calculated by comparing the difference of each onset temperature in the heating T_{onset}(heating) and cooling T_{onset}(cooling) curve.

$$\Delta T = T_{\text{onset}}(\text{heating}) - T_{\text{onset}}(\text{cooling}) \quad (2)$$

Generally, the degree of undercooling is proportional to the amount of Sn in the solder. Besides, the addition of small amounts of alloying elements to solders tends to be associated with small undercooling, since such elements may serve as extra heterogeneous nucleation sites and promote the solidification process [10,11]. However, a new finding is observed in DSC analysis. Although the degree of undercooling appears to be dependent on the amount of Cu in Sn–6.5Zn solder, the onset temperature during cooling (T_{onset}) not appeared at lower temperature, but at higher temperature compared to the onset temperature during heating (T_{onset}). With such abnormal continuous compositional change, the equilibrium solidification temperatures of solders are not specified, and the degrees of undercooling cannot be determined according to the above definition, since the change of equilibrium solidification temperatures is caused by the variation of nucleation ability of primary solidification Zn and γ-Cu_5Zn_8 phases. As an approximation, the liquidus temperature during heating was assumed to be the equilibrium solidification temperature as reported by Huang et al. [16]. Based on this assumption, the equilibrium solidification temperature during heating for Sn–6.5Zn–0.5Cu and Sn–6.5Zn–1.5Cu solders are at 204.3 and 217.5 °C, respectively. Since the T_{onset} during cooling are 203.3 °C and 208.9 °C for two solders, respectively, the degree of undercooling can be determined to be 1 °C and 8.6 °C for Sn–6.5Zn–0.5Cu and Sn–6.5Zn–1.5Cu solders, respectively. Consistent with XRD analysis shown in Fig. 4, it is assumed that addition of Cu atoms not only substitute at Zn sites to form γ-Cu_5Zn_8 IMCs in the molten solder, but also precipitates during cooling to form small particles that may be considered as a primary phase. Once the solidification process begins, the degrees of undercooling can be related to the nucleation ability of γ-Cu_5Zn_8 within the melt. Nevertheless, the primary phases may not have provided suitable sites for heterogeneous nucleation. As a result, the degree of undercooling increases with increasing Cu content. Recently, Liu et al. [17] examined the degree of undercooling in Sn–Pb solders with changing the amount of Pb. In agreement with the present results, not only the degree of undercooling was found to be proportional to the amount of Pb in Sn–Pb solders, but also the onset temperature during cooling appeared at higher temperature than the onset temperature during heating. Their results indicate that Pb is the element that nucleates at higher temperature, while Sn phase nucleates at lower temperature.

3.2. Microstructure of Sn–6.5Zn–xCu alloys

To identify the initial phases, the as-solidified alloys were examined by XRD, as shown Fig. 4. The microstructure

Table 2
Solidus temperature (T_{onset}), liquidus temperature (T_{end}), Pasty range, (T_{onset}) during cooling, undercooling range and Peak temperature for Sn–6.5Zn, Sn–6.5Zn–0.5Cu and Sn–6.5Zn–1.5Cu solder alloys.

Alloy	(T_{onset}) (°C) heating	(T_{end}) (°C) heating	Pasty range (T_{end}–T_{onset}) (°)	(T_{onset}) cooling	Undercooling (°C)	Peak temperature (°C)	
						P_1	P_2
Sn–6.5Zn	197.8	204.2	6.4	197	0.8	200.5	–
Sn–6.5Zn–0.5Cu	197.6	204.3	6.7	203.3	1.0	200.6	–
Sn–6.5Zn–1.5Cu	197.0	217.5	20.5	208.9	8.6	200.6	214.6

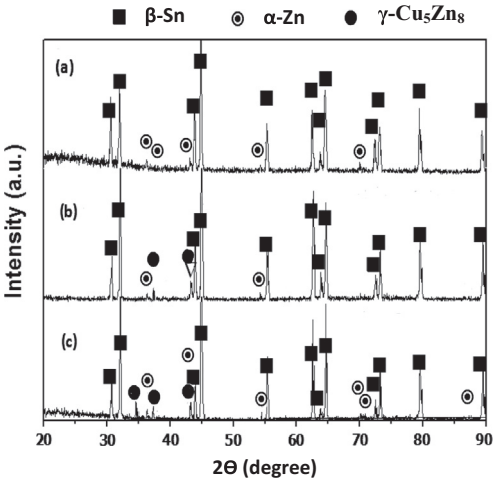

Fig. 4. XRD analysis of as-solidified (a) Sn–6.5Zn, (b) Sn–6.5Zn–0.5Cu and (c) Sn–6.5Zn–1.5Cu solder alloys.

of Sn–6.5Zn alloy consists of (i) β-Sn and (ii) α-Zn-rich phase. According to the Sn–Zn, binary phase diagram, there is no IMC formed during solidification process and Zn phase could precipitate as a separate phase due to its lower solubility in Sn (about 0.4 wt.% at 180 °C). With the addition of Cu, the microstructures of ternary alloys can be distinguished into three phases, *i.e.* (i) β-Sn and (ii) α-Zn and (iii) γ-Cu_5Zn_8 IMC. The SEM observations (Fig. 5a) show that the acicular shaped α-Zn phase was homogeneously distributed in β-Sn matrix. Size distributions of light contrast β-Sn and dark needle-like α-Zn-rich phase are close to the typical eutectic Sn–9Zn structure [18]. However, the precipitation of large number of undesirable primary α-Zn phase is well known to degrade the mechanical properties of Sn–Zn solder owing to the brittleness of Zn. For 0.5% Cu-containing specimens (Fig. 5b), the needle-like α-Zn morphology was remarkably suppressed after Cu modification, and dramatically changed to both fine particles and some relatively fine needle-like Zn-rich phase. In addition, a new type of dark flower-like γ-Cu_5Zn_8 IMC was detected for 0.5 wt.% Cu added specimens. A possible reason for the finer Zn-rich phase could be related to consumption of Zn due to γ-phase formation. As the Cu content increases, the α-Zn phase becomes finer with needle structure, but a large number of coarse dendrite-like structures of γ-Cu_5Zn_8 phase were observed (Fig. 5c). From the EDS profile and elemental analysis of large γ-Cu_5Zn_8 particles shown in Fig. 6, the dark phase consisted of Cu and Zn, and the percentage of Cu was about 35.87 wt.%. This statement implies that the dark phase may be γ-Cu_5Zn_8 phase.

3.3. General tensile tests

Mechanical properties play a crucial role in the metallurgical bond for Pb-free solder alloys. The general tensile properties of Sn–6.5Zn, Sn–6.5Zn–0.5Cu and Sn–6.5Zn–1.5Cu alloys at $T = 25$ °C and strain rate of 2.9×10^{-3} s^{-1} are shown in Fig. 7. The experimental results point to some exclusive features for the tensile behavior of solders. The tensile specimens of Sn–6.5Zn–*x*Cu solders experience simultaneous work hardening and dynamic recovery when they are deformed, as reported by El-Daly et al. [10]. The former hardens the solders, while the latter leads to strain softening caused by thermal activated process owing to the low T_m of Sn–6.5Zn–*x*Cu solders. Consequently, the resolved stress–strain curves exemplify the combined effects of both factors. However, Fig. 8 shows the comparative tensile stress–strain curves for three alloys at (a) $T = 25$ and (b) $T = 70$ °C with strain rate of 1.15×10^{-3} s^{-1}. The ultimate tensile strength (UTS), yield stress (0.2%YS), Young's modulus and elongation (El.%) are assembled in the corresponding histogram. It is seen that the stress levels decreased with increasing temperature at constant strain rate, whereas the elongation is decreased and increased with inconsistent behavior. However, these results are in good agreement with the previous findings [10] that the tensile behavior of Sn–6.5Zn alloy often exhibits strain rate and temperature dependence. Table 3 exemplified that the UTS and Young's modulus of Sn–6.5Zn–0.5Cu solder are

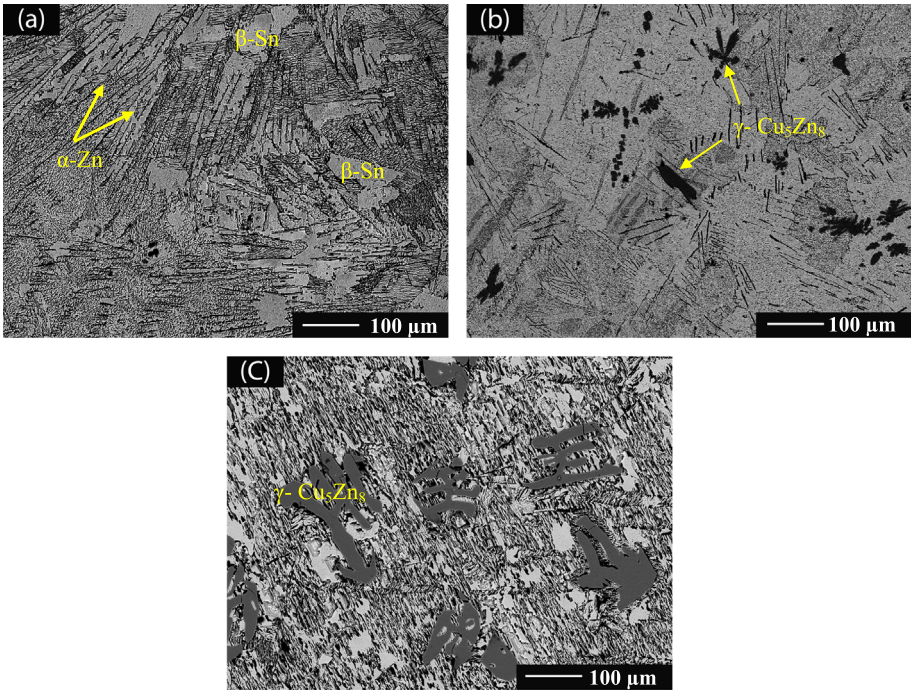

Fig. 5. Low-magnification SEM microstructures of (a) Sn–6.5Zn, (b) Sn–6.5Zn–0.5Cu and (c) Sn–6.5Zn–1.5Cu solder alloys.

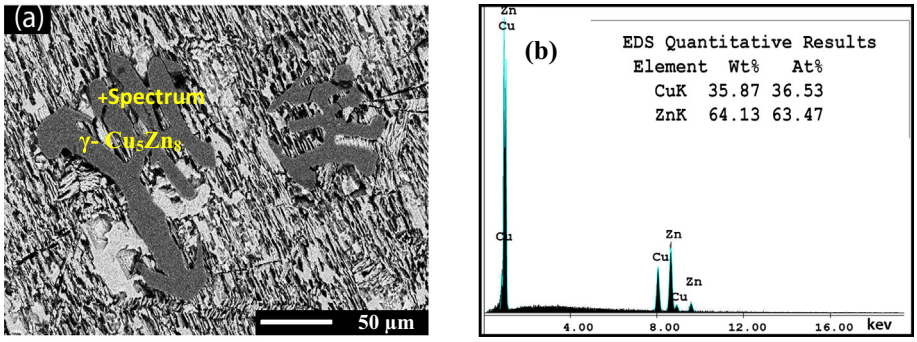

Fig. 6. High-magnifications SEM microstructure of Sn–6.5Zn–1.5Cu alloy and corresponding EDS analysis of γ-Cu_5Zn_8.

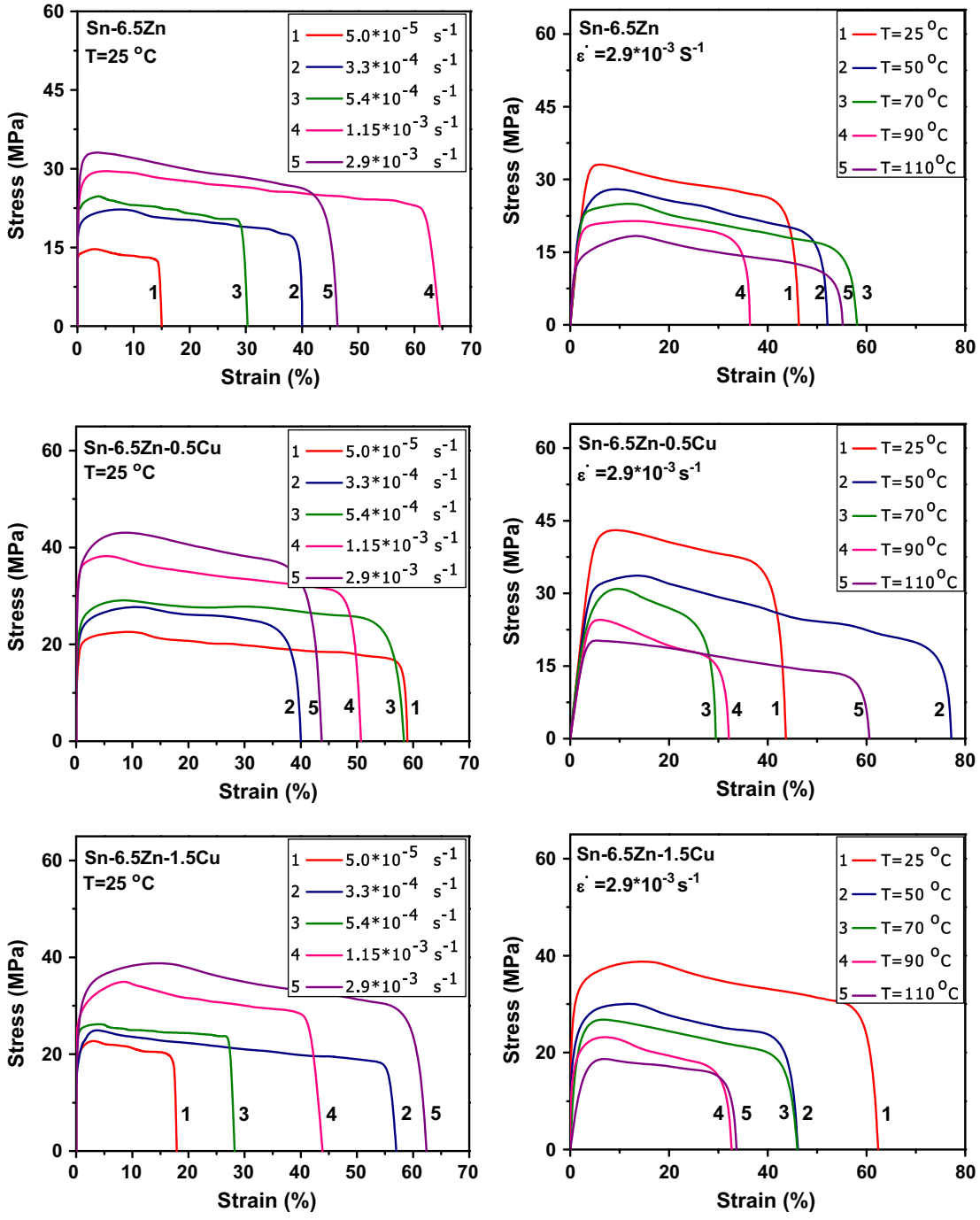

Fig. 7. General tensile properties of Sn–6.5Zn, Sn–6.5Zn–0.5Cu and Sn–6.5Zn–1.5Cu solder alloys at $T = 25$ °C and strain rate of 2.9×10^{-3} s^{-1}.

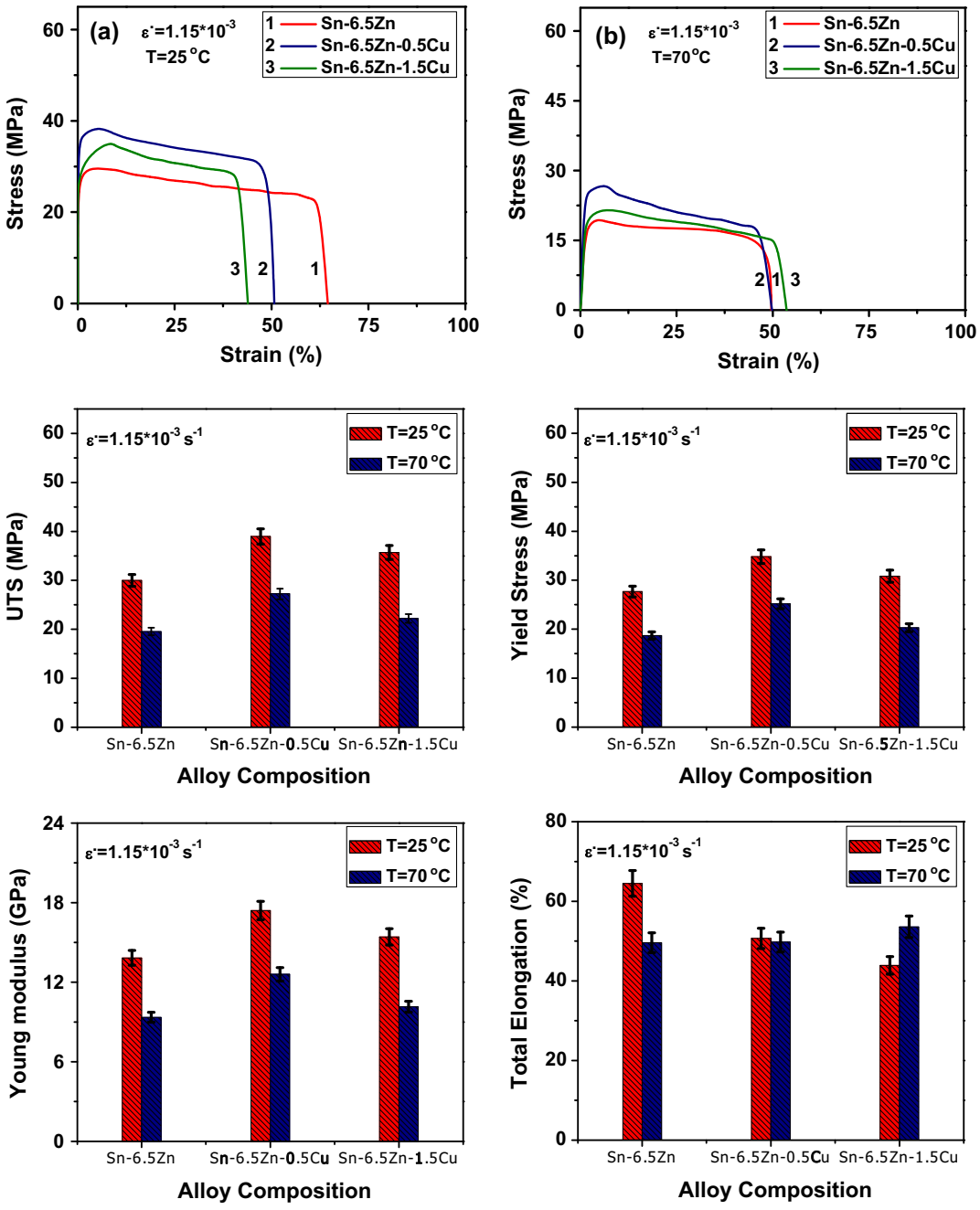

Fig. 8. Comparative tensile curves at (a) $T = 25$ °C and (b) $T = 70$ °C at $\dot{\varepsilon} = 1.15 \times 10^{-3}$ s^{-1} for Sn–6.5Zn, Sn–6.5Zn–0.5Cu and Sn–6.5Zn–1.5Cu solder alloys and corresponding histogram of: ultimate tensile strength (UTS), yield stress (YS), Young's modulus and elongation (El.%).

Table 3
Tensile properties of the solders Sn–6.5Zn, Sn–6.5Zn–0.5Cu and Sn–6.5Zn–1.5Cu solder alloys at $T = 25$ °C and $\dot{\varepsilon} = 1.15 \times 10^{-3}$ s^{-1}.

Alloy	UTS (MPa)	YS (MPa)	Elongation (%)	Young's modulus (GPa)
Sn–6.5Zn	30.0 ± 3	27.7 ± 2	64.5 ± 5	13.8 ± 2
Sn–6.5Zn–0.5Cu	39.0 ± 3	34.8 ± 2	50.7 ± 5	17.4 ± 2
Sn–6.5Zn–1.5Cu	35.7 ± 3	30.8 ± 2	43.9 ± 5	15.4 ± 2

respectively, 39.0 MPa and 17.4 GPa, higher than 30.0 MPa and 13.8 GPa of Sn–6.5Zn solder, whereas the ductility of Sn–6.5Zn–0.5Cu solder is only 12.3% lower than the plain solder. Conversely, the addition of 1.5% Cu has a little influence on the tensile strength and Young's modulus of Sn–6.5Zn solder. But the elongation of the Sn–6.5Zn solder deteriorates remarkably after 1.5% Cu addition. The improvement in both tensile strength and ductility of Sn–6.5Zn–*x*Cu solders is mainly depend on the shape and size of phase structure, and composition of alloy solders, which played a significant role for controlling the mechanical behavior.

3.4. Effect of strain rate on the mechanical properties

The effect of strain rate $\dot{\varepsilon}$ on ultimate tensile strength (UTS), yield stress (YS), Young modulus and elongation (El.%) of Sn–6.5Zn–*x*Cu solders at $T = 25$ °C is shown in Fig. 9. The results indicate that the measured UTS values grew by more than 30% for each strain rate increase. Nevertheless, the ductility of three solders as articulated by elongation exhibits random increase with increasing strain rate, specifying that the true strain rate had a slight effect on the ductility of specimens in strain rate range investigated. On the other hand, the mechanical strength is improved by adding appropriate amount of Cu and the peak value acquired with 0.5 wt.% Cu addition, as summarized in Table 4. Although the 1.5 wt.% Cu addition can produce larger dendrites γ-Cu_5Zn_8 IMC phase, which lead to weakening in tensile strength, the observed increase of mechanical strength of 0.5Cu containing solder suggests that the existence of finer α-Zn and γ-Cu_5Zn_8 particles in analogy to the Hall–Petch relation of grain strengthening. However, for both plain and Cu doped solders, the flow stresses show strong positive dependence on strain rate, indicating that the flow stresses increase as the strain rate increases.

3.5. Effect of temperature on the mechanical properties

The increment of temperature is precious for reducing critical YS, UTS, and Young's modulus as well as extended the slipping and diffusion ability of atoms at interfaces. The temperature dependence of tensile stress–strain curves of three solders at initial strain rate of 2.9×10^{-3} s^{-1} is seen in Fig. 10. The results are summered in Table 5. For Sn–6.5Zn alloy, the UTS, YS and Young's modulus exhibit the values of 31.6 MPa, 33.9 MPa and 15.8 GPa at room temperature, respectively. With the increment of deformation temperature, the UTS, YS and Young's modulus are gradually decreased to 16.9 MPa, 19.0 MPa and 8.4 GPa, respectively. The variation tendency of UTS and YS may be due to the dynamic recovery process, which is more significant during elevation of temperature. The alloy composition is another important parameter in influencing the tensile parameters of solder samples. The substantial observation made during tensile tests is that the highest UTS, YS and Young's modulus appeared with the Sn–6.5Zn–0.5Cu alloy samples followed by the Sn–6.5Zn–1.5Cu and Sn–6.5Zn alloys. For instance, the UTS of Sn–6.5Zn increases

Table 4
Mechanical property data for different solders at temperature 25 °C and various strain rates.

Alloy/$\dot{\varepsilon}$	UTS (MPa)	YS (MPa)	Elongation (%)	Young's modulus (GPa)
Sn–6.5Zn				
$5.0 * 10^{-5}$ s^{-1}	14.9	13.5	15.1	6.8
$3.3 * 10^{-4}$ s^{-1}	22.8	20.1	40.2	10.1
$5.4 * 10^{-4}$ s^{-1}	24.9	23.5	30.3	11.8
$1.15 * 10^{-3}$ s^{-1}	30.0	27.7	64.5	13.8
$2.9 * 10^{-3}$ s^{-1}	33.9	31.6	46.3	15.8
Sn–6.5Zn–0.5Cu				
$5.0 * 10^{-5}$ s^{-1}	22.9	20.6	59.1	10.3
$3.3 * 10^{-4}$ s^{-1}	28.4	24.3	40.1	12.1
$5.4 * 10^{-4}$ s^{-1}	29.6	26.5	58.4	13.2
$1.15 * 10^{-3}$ s^{-1}	39.0	34.8	50.7	17.4
$2.9 * 10^{-3}$ s^{-1}	44.6	38.7	43.7	19.3
Sn–6.5Zn–1.5Cu				
$5.0 * 10^{-5}$ s^{-1}	23.1	20.6	17.9	10.3
$3.3 * 10^{-4}$ s^{-1}	257	21.8	57.1	10.9
$5.4 * 10^{-4}$ s^{-1}	26.4	24.8	28.2	12.4
$1.15 * 10^{-3}$ s^{-1}	35.7	30.8	43.9	15.4
$2.9 * 10^{-3}$ s^{-1}	39.4	34.1	62.4	17.1

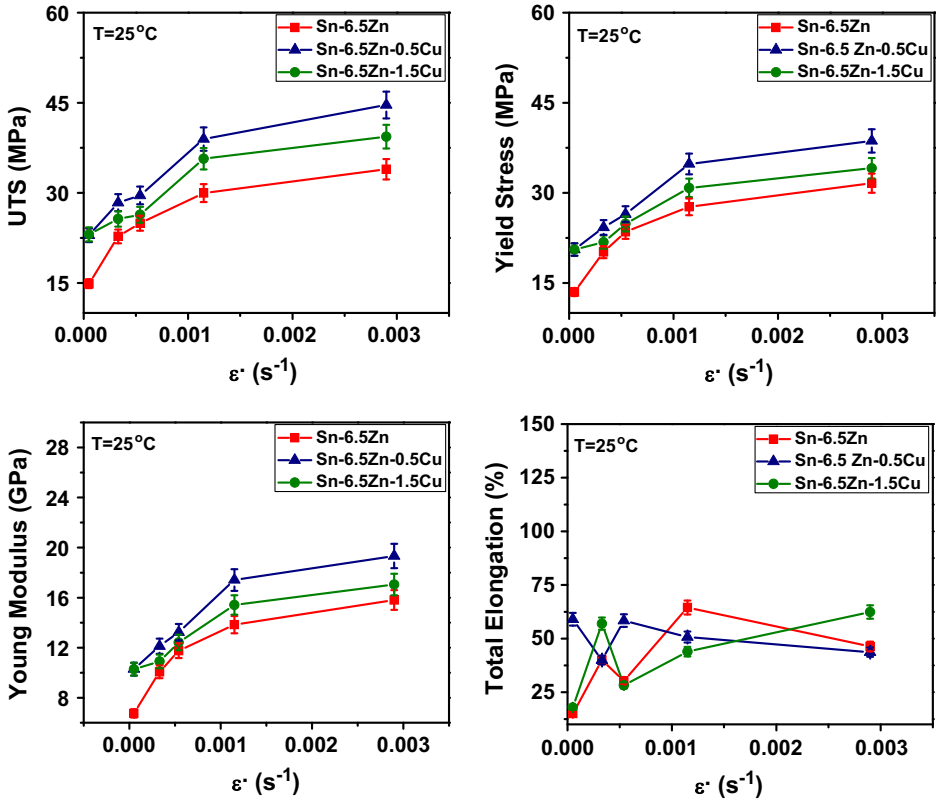

Fig. 9. Effect of strain rate on: ultimate tensile strength (UTS), yield stress (YS), Young modulus and elongation (El.%) at $T = 25$ °C for Sn–6.5Zn, Sn–6.5Zn–0.5Cu and Sn–6.5Zn–1.5Cu solder alloys.

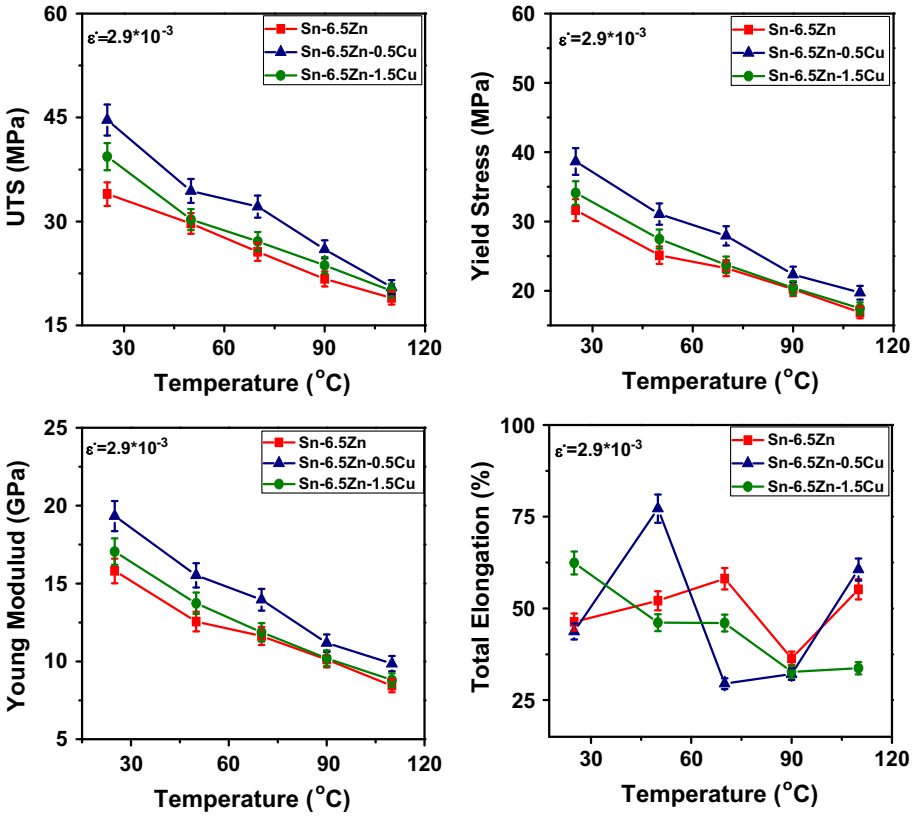

Fig. 10. Effect of temperature on: ultimate tensile strength (UTS), yield stress (YS), Young modulus and elongation (El.%) at $T = 25$ °C for Sn–6.5Zn, Sn–6.5Zn–0.5Cu and Sn–6.5Zn–1.5Cu solder alloys.

Table 5
Mechanical property data for different solders at $\dot{\varepsilon} = 2.9 \times 10^{-3}\ s^{-1}$ and different temperatures.

Alloy/temp. (°C)	UTS (MPa)	YS (MPa)	Elongation (%)	Young modulus (GPa)
Sn–6.5Zn				
25 °C	33.9	31.6	46.3	15.8
50 °C	29.7	25.1	52.1	12.6
70 °C	25.6	23.3	58.1	11.6
90 °C	21.7	20.2	36.4	10.1
110 °C	19.0	16.9	55.2	8.4
Sn–6.5Zn–0.5Cu				
25 °C	44.6	38.7	43.7	19.3
50 °C	34.4	31.1	77.2	15.5
70 °C	32.1	27.9	29.5	14.1
90 °C	26.0	22.4	32.1	11.2
110 °C	20.5	19.7	60.6	9.9
Sn–6.5Zn–1.5Cu				
25 °C	39.4	34.1	62.4	17.1
50 °C	30.3	27.5	46.1	13.7
70 °C	27.1	23.7	46	11.9
90 °C	23.7	20.4	32.7	10.2
110 °C	20.0	17.5	33.7	8.8

from 33.9 to 44.6 MPa with the addition of 0.5% Cu, while 1.5% Cu addition has little significant effect on the UTS of Sn–6.5Zn (39.4 MPa). The improvement in tensile parameters with the addition of 0.5Cu solder may be attributed to two reasons: One is the change of α-Zn morphology from large needle-shaped precipitates to both fine α-Zn particles and some relatively fine needle-like Zn-rich phase, which is effectively contribute to block the dislocation movement initiated in the ductile β-Sn phase of Sn–6.5Zn–0.5Cu solder. Another is the formation of additional type of flower-like γ-Cu_5Zn_8 IMC, However, the shrinking of mechanical strength with the addition of 1.5Cu could result in the observed coarsening of γ-Cu_5Zn_8 phase inside the alloy matrix. The elongation was found to increase and decreases with irregular behavior for all solder alloys. The comparison of ductility for three solders indicates the better performance of Sn–6.5Zn–0.5Cu solder, as realized from its higher level of elongation when considered at most temperature and strain rate levels. These results also imply that high positive strain rate sensitivities are necessary to produce high plasticity at certain strain rate and temperature. Several possible reasons are established for ductility sensitivity to the testing temperatures such as grain size, compositional effects on matrix phase and IMC chemistries, the stability of soft and hard IMCs in the alloy matrix, variation of stress exponent with temperature [19].

3.6. Constitutive equations

For lead-free solders, a noticeable linear relationship is accounted between tensile strength and strain rate in double logarithmic coordinates. The most comprehensive way of analyzing the deformation behavior incorporates both the stress exponent n and activation energy Q values. The data are generally analyzed in two ways:

(a) The standard power-law equation, which is an extension of Eq. (3) and includes the Arrhenius term [20,21]:

$$\dot{\varepsilon} = A\sigma^n \exp(-Q/RT) \tag{3}$$

(b) Garafalo hyperbolic sine equation [11]:

$$\dot{\varepsilon} = A[\sinh(\alpha\sigma)]^n \exp(-Q/RT) \tag{4}$$

where A is the material constant, R is the gas constant ($R = 8.314$ J/mol K) and α is the stress multiplier and signifies the

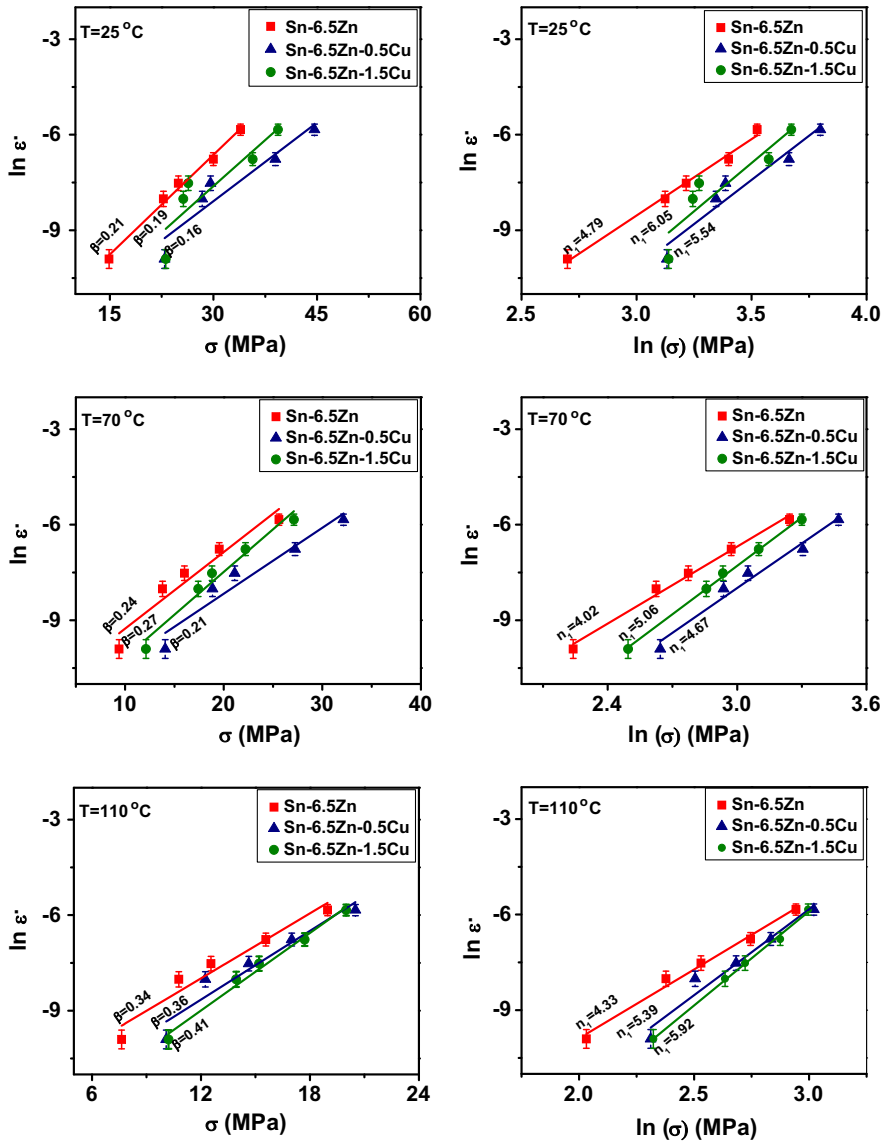

Fig. 11. Relationship between σ, $\ln(\dot{\varepsilon})$ and $\ln(\sigma$ (, $\ln(\dot{\varepsilon})$ at $T = 25$, 70 and 110 °C for Sn–6.5Zn, Sn–6.5Zn–0.5Cu and Sn–6.5Zn–1.5Cu solder alloys.

stress reciprocal at which the material deformation changes from power to exponential stress dependence. For clarifying the deformation behavior over a wide range of temperature T and strain rate $\dot{\varepsilon}$, more attention is paid to the minimum strain rate which can be expressed by hyperbolic-sine law. The value of α can be described as $\alpha = \beta/n_1$, where β and n_1 are the average slopes of $\ln(\dot{\varepsilon}) - \sigma$ and $\ln(\dot{\varepsilon}) - \ln(\sigma)$ lines, respectively, as seen in Fig. 11. Hence, the values n are determined from the slope of $\ln\dot{\varepsilon}$ against $\ln[\sinh(\alpha\sigma)]$ plot in the temperature range of 25–110 °C (Fig. 12). The Q value can be expressed as the slope of $\ln[\sinh(\alpha\sigma)]$ against $1/T$ (Fig. 13). The results of hyperbolic sine relationship are given in Table 6.

As seen in Table 6, the power law is verified and the stress exponent values are slightly reduced with increasing temperature in all temperature range investigated. The n values are decreased from 4.3 to 3.9, 5.0 to 4.1, and 4.7 to 4.2 as the temperature increases from 25 to 110 °C for Sn–6.5Zn, Sn–6.5Zn–0.5Cu and Sn–6.5Zn–1.5Cu solders, respectively. The slight change of n values reflects the stability of microstructure at high temperatures and the sensitivity of Sn–6.5Zn to Cu addition. It is worth noting that Sn–6.5Zn–0.5Cu alloy exhibits higher n-values than the other alloys. However, the higher the stress exponent is, the better the strengthening effect of alloy matrix. This is assumed to be a result of microstructural changes due to the refinement of fine needle-like Zn-rich phase and presence of γ-Cu_5Zn_8 IMC particles. Fine uniform dispersions of γ-Cu_5Zn_8 IMCs could enhance the thermal stability of alloy samples. The dispersions influence nearly all the tensile mechanisms owing to dislocations. These fine IMC particles could act as a sources and sinks of vacancies for diffusion mechanisms, which accommodate the climb of dislocations when they encounter the second phase particles. Generally, the tensile deformation mechanisms of interest are classified by their stress exponent value from smallest to largest: The stress exponent 2 is associated with grain-boundary-sliding-type alloys, 3 for solid solution alloys and from 4 to 7 for dispersion strengthened alloys [13,22]. In Sn–6.5Zn alloys, the n values are close to the stress exponents of pure metals, in which the tensile behavior is controlled by dislocation climb related processes. The enhancement in tensile strength with the addition of 0.5 wt.% of Cu can be attributed to the interactions of dislocations with the γ-Cu_5Zn_8 IMC particles, which hinder the climb of dislocations. Other similar results obtained by tensile testing of Sn–6.5Zn alloys indicate n values in the range of 4.1–7.5 at temperature range of 25–110 °C [10]. The apparent activation energy of about 46.7, 62.3 and

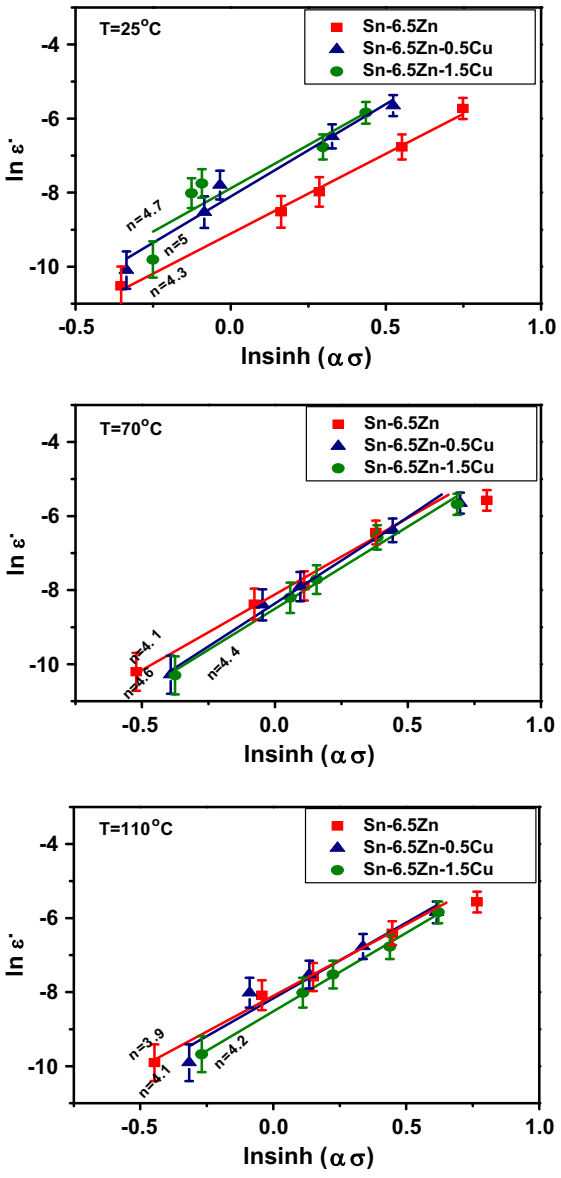

Fig. 12. Relationship between $\ln[\sinh(\alpha\sigma)]$ and $\ln(\dot{\varepsilon})$ for calculation stress exponent (n) values at $T = 25$, 70 and 110 °C of Sn–6.5Zn, Sn–6.5Zn–0.5Cu and Sn–6.5Zn–1.5Cu solder alloys.

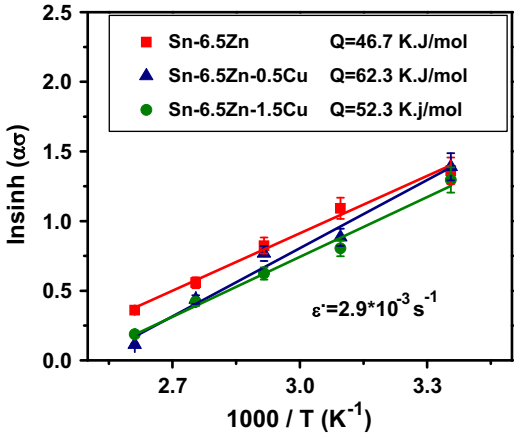

Fig. 13. The activation energy (Q) values of Sn–6.5Zn, Sn–6.5Zn–0.5Cu, Sn–6.5Zn–1.5Cu solder alloys.

Table 6
Activation energy (Q) and stress exponent (n) values for Sn–6.5Zn, Sn–6.5Zn–0.5Cu and Sn–6.5Zn–1.5Cu solder alloys.

Alloy	Q (kJ/mol)	Temperature (°C)	α	n
Sn–6.5Zn	46.7	25	0.044	4.3
		70	0.06	4.1
		110	0.079	3.9
Sn–6.5Zn–0.5Cu	62.3	25	0.029	5.0
		70	0.045	4.6
		110	0.067	4.1
Sn–6.5Zn–1.5Cu	52.3	25	0.031	4.7
		70	0.053	4.4
		110	0.069	4.2

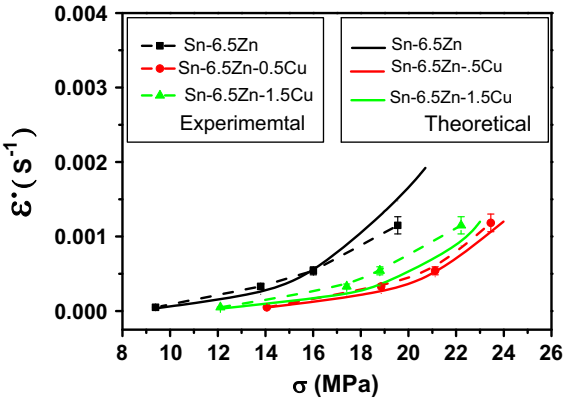

Fig. 14. Comparison of strain rate achieved from experimental results and Garofalo model at70 °C.

52.3 kJ mol^{-1} were obtained for Sn–6.5Zn, Sn–6.5Zn–0.5Cu and Sn–6.5Zn–1.5Cu solders, respectively, which are somewhat close to that of dislocation pipe diffusion [19,23]. The slight observed difference in the n and Q values could be due to the variation of microstructures in the present solder alloys. Hence, it is proposed that the operative tensile mechanism in all tested alloys is dislocation climb controlled by dislocation pipe diffusion. Remarkably, the Q value of Sn–6.5Zn–0.5Cu solder is higher than the other alloys, since the fine dispersion of γ-Cu_5Zn_8 IMCs contributing to effective distance for dislocation movement [10]. The activation energy term is associated with the binding energy between the dislocations and obstacles. The high dislocation density due to γ-Cu_5Zn_8 IMCs suggests that dislocation pipe diffusion may provide a short circuit for diffusion, which in turn authorizes the rapid dislocation climb to move under high applied strain rates. The data obtained from the present results indicate that the alloy samples exhibit a nearly identical strain rate to that of pure Sn, but can operate at higher stress than in pure Sn. The combined effect of strain rate and temperature on deformation processes can be modeled by exponent type equations for Sn–6.5Zn, Sn–6.5Zn–0.5Cu and Sn–6.5Zn–1.5Cu solder alloys. Conversely, the experimental data of A, Q, n and α were assembled for three solder alloys, and fitted with Garofalo hyperbolic sine Law as follows:

$$\dot{\varepsilon} = 2.88 \times 10^{-4}[\sinh(0.061\sigma)]^{4.1} \exp\left(\frac{-46.7}{RT}\right) \quad (5)$$

$$\dot{\varepsilon} = 2.34 \times 10^{-4}[\sinh(0.047\sigma)]^{4.6} \exp\left(\frac{-62.3}{RT}\right) \quad (6)$$

$$\dot{\varepsilon} = 2.1 \times 10^{-4}[\sinh(0.051\sigma)]^{4.4} \exp\left(\frac{-52.3}{RT}\right) \quad (7)$$

Fig. 14 compares the Garofalo model (Eqs. (5)–(7)) with the experimental results for strain rate versus stress behavior at 70 °C. The comparison of these results gives a good fit for strain rate versus stress data at some temperature for the three solder alloys.

4. Conclusions

In this study, effects of Cu addition on microstructure, thermal behavior and tensile properties of Sn–6.5Zn based alloys have been investigated. The results are summarized as follows:

(1) Addition of 0.5% Cu into plain Sn–6.5Zn solder leads to formation of new type of dark flower-like γ-Cu_5Zn_8 IMC and reducing the amount of large needle-shaped Zn phase, while the addition of 1.5%Cu leads to creation of coarse dendrite-like morphology of γ-Cu_5Zn_8 phase.
(2) The amount of Cu addition has been found to control the melt crystallization of Sn–6.5Zn solder. Small amount of Cu has no effect on eutectic temperature, pasty range and undercooling of Sn–6.5Zn solder, which can improve the soldering properties in electronic packaging whereas, the large amount of Cu induced undesirable effects on both eutectic temperature, pasty range and undercooling, which can cause a lot of manufacturing problems.
(3) Based on the experimental observations, the highest experimental UTS and YS results are that of Sn–6.5Zn–0.5Cu solder followed by those of Sn–6.5Zn–1.5Cu alloy with intermediate values and lowest values exhibited by the traditional Sn–6.5Zn alloy.
(4) The average stress exponents lie in the range of 3.9–5.0. These stress exponents together with the activation energies, which are close to 46.7–62.3 kJ mol^{-1} for dislocation pipe diffusion of Sn, suggest that the operative deformation mechanism is dislocation climb controlled by dislocation pipe diffusion.
(5) Garofalo model is suitable for describing the experimental flow behavior of Sn–6.5Zn solder solders over the strain rate and temperature range investigated.

References

[1] C.H. Wang, H.-H. Chen, P.-Y. Li, P.-Y. Chu, Kinetic analysis of Ni_5Zn_{21} growth at the interface between Sn–Zn solders and Ni, Intermetallics 22 (2012) 166–175.
[2] A.A. El-Daly, W.M. Desoky, T.A. Elmosalami, M.G. El-Shaarawy, A.M. Abdraboh, Microstructural modifications and properties of SiC nanoparticles-reinforced Sn–3.0Ag–0.5Cu solder alloy, Mater. Des. 65 (2015). 1196–04.
[3] L.C. Tsao, R.W. Wu, T.-H. Cheng, K.-H. Fan, R.S. Chen, Effects of nano-Al_2O_3 particles on microstructure and mechanical properties of Sn3.5Ag0.5Cu composite solder ball grid array joints on Sn/Cu pads, Mater. Des. 50 (2013) 774–781.
[4] L. Zhang, Xue Gao, S.-B. Li-li, Z. Sheng, H. Ye, Z.-X. Xiao, G. Zeng, et al., Development of Sn–Zn lead-free solders bearing alloying elements, J. Mater. Sci.: Mater. Electron. 21 (2010) 1–15.
[5] A.A. El-Daly, A.E. Hammad, Effects of small addition of Ag and/or Cu on the microstructure and properties of Sn–9Zn lead-free solders, Mater. Sci. Eng., A 527 (2010) 5212–5219.
[6] L.R. Garcia, W.R. Osório, L.C. Peixoto, G. Amauri, Mechanical properties of Sn–Zn lead-free solder alloys based on the microstructure array, Mater. Charact. 61 (2010) 212–220.
[7] C.-Y. Liu, M.-H. Hon, M.-C. Wang, Y.-R. Chen, K.-M. Chang, W.-L. Li, Effects of aging time on the mechanical properties of Sn–9Zn–1.5Ag–*x*Bi lead-free solder alloys, J. Alloys Compd. 582 (2014) 229–235.
[8] T.B. Massalski, Editor-in-Chief, Binary Alloy Phase Diagrams, second ed., vol. 2, ASM International, Ohio, 1992, p.3416.
[9] X. Wei, H. Huang, L. Zhou, M. Zhang, X. Liu, On the advantages of using a hypoeutectic Sn–Zn as lead-free solder material, Mater. Lett. 61 (2007) 655–658.
[10] A.A. El-Daly, A.E. Hammad, G.A. Al-Ganainy, A.A. Ibrahiem, Design of lead-free candidate alloys for low-temperature soldering applications based on the hypoeutectic Sn–6.5Zn alloy, Mater. Des. 56 (2014) 594–603.
[11] A.A. El-Daly, A.E. Hammad, G.A. Al-Ganainy, A.A. Ibrahiem, Enhancing mechanical response of hypoeutectic Sn–6.5Zn solder alloy using Ni and Sb additions, Mater. Des. 52 (2013) 966–973.
[12] P. Zimprich, U. Saeed, A. Betzwar-kotas, B. Weiss, H. Ipser, Mechanical size effects in miniaturized lead-free solder joints, J. Electron. Mater. 37 (2008) 102–109.
[13] S. Wiese, M. Roellig, M. Mueller, K.-J. Wolter, The effect of downscaling the dimensions of solder interconnects on their creep properties, Microelectron. Reliab. 48 (2008) 843–850.
[14] A.A. El-Daly, A.E. Hammad, Enhancement of creep resistance and thermal behavior of eutectic Sn–Cu lead-free solder alloy by Ag and In-additions, Mater. Des. 40 (2012) 292–298.
[15] G. Saad, S.A. Fayek, A. Fawzy, H.N. Soliman, Gh. Mohammed, Deformation characteristics of Al-4043 alloy, Mater. Sci. Eng., A 527 (2010) 904–910.
[16] Y.-C. Huang, S.-W. Chen, K.-S. Wu, Size and substrate effects upon undercooling of Pb-free solders, J. Electron. Mater. 39 (2010) 109–114.
[17] Y. Liu, Z. Chen, J.N. Wang, Large undercooling rapid solidification and nucleation mechanism in multi-stage atomization, Sci. Technol. Adv. Mater 1 (2001) 181–184.
[18] A.A. El-Daly, Y. Swilem, M.H. Makled, M.G. El-Shaarawy, A.M. Abdraboh, Thermal and mechanical properties of Sn–Zn–Bi lead-free solder alloys, J. Alloys Compd. 484 (2009) 134–142.
[19] R. Mahmudi, A.R. Geranmayeh, H. Khanbareh, N. Jahangiri, Indentation creep of lead-free Sn–9Zn and Sn–8Zn–3Bi solder alloys, Mater. Des. 30 (2009) 574–580.
[20] Z. Jing, C. Boquan, B. Zhang, Effect of initial microstructure on the hot compression deformation behavior of a 2219 aluminum alloy, Mater. Des. 34 (2012) 15–21.
[21] V. Senthilkumar, A. Balaji, R. Narayanasamy, Analysis of hot deformation behavior of Al 5083–TiC nanocomposite using constitutive and dynamic material models, Mater. Des. 37 (2012) 102–110.
[22] Y. Kanda, Y. Kariya, Evaluation of creep properties for Sn–Ag–Cu micro solder joint by multi-temperature stress relaxation test, Microelectron. Reliab. 52 (2012) 1435–1440.
[23] R. Mahmudi, A.R. Geranmayeh, H. Noori, M. Taghaddosi, Effects of Ag and Al additions on the structure and creep properties of Sn–9Zn solder alloy, J. Electron. Mater. 38 (2009) 330–337.